

LONG-SLIT SPECTROSCOPY IN THE ROCKET ULTRAVIOLET OF THE ORION NEBULA

RALPH C. BOHLIN

Laboratory for Astronomy and Solar Physics, Goddard Space Flight Center

JESSE K. HILL

Systems and Applied Sciences Corporation

THEODORE P. STECHER

Laboratory for Astronomy and Solar Physics, Goddard Space Flight Center

AND

ADOLF N. WITT

Ritter Astrophysical Research Center, University of Toledo

Received 1979 November 19; accepted 1980 January 9

ABSTRACT

Ultraviolet spectra of the Orion Nebula were obtained with a rocket-borne telescope in three 1 minute exposures by using a microchannel plate detector and film. The slit, 17' long and 22" wide, was centered on a line passing near θ^2 Orionis B and through a point 38" northeast of the Trapezium star θ^1 Orionis C. The relative intensities from the rocket were placed on the *IUE* absolute flux scale by using an *IUE* spectrum of θ^2 Ori B. In addition to the spectrum of θ^2 Ori B, the rocket data consist of the spectrum of the nebula, which we divide into three parts for discussion: a "bar" near θ^2 Ori B, the "inner nebula" near the Trapezium, and the "faint nebula" further from the Trapezium.

Three emission lines are present in each part of the nebula, the C III] intercombination doublet at 1908 Å, the C II] intercombination line at 2326 Å and the [O II] forbidden doublet at 2470 Å. The absolute intensities of the lines are tabulated and a simple determination gives a C/O abundance ratio of unity, compared to 0.5 in the Sun.

The continuum is produced primarily by the scattering of starlight from θ^1 Ori C on the dust particles in the nebula. There is a small atomic component present in the continuum, which is only significant at the longer wavelengths. For the three parts of the nebula observed, we present the relative nebular surface brightness expressed as $\log (S/F)_\lambda$, where F is the flux from θ^1 Ori C as measured by *IUE*. In all three ratios of (S/F) , the 2200 Å extinction feature is small. The inner nebula is bluer than the star at the shorter wavelengths, and the bar is neutral in color, while the faint nebula is redder than the star at shorter wavelengths. We discuss the implications of these ratios of (S/F) in terms of the grain albedo and scattering properties.

Subject headings: nebulae: abundances — nebulae: Orion Nebula — spectrophotometry — ultraviolet: spectra

1. INTRODUCTION

Of all the diffuse nebulae, NGC 1976, the Orion Nebula, is the most studied H II region in the sky with more than a score of papers appearing on it each year. The Orion Nebula has high surface brightness, low foreground extinction, and sufficient angular extent to make it ideal for exploratory spectroscopy in the ultraviolet. The Orion Nebula is the ionized portion of a large neutral molecular cloud. Star formation has recently occurred in the front part of this cloud and the most massive star, θ^1 Orionis C, is producing most of the ionization. In the UV the principal source of emission from the nebula is starlight scattered from the dust grains. Few emission lines are present, because the temperature of the gas in H II regions is too cool to

strongly populate the atomic levels that produce UV lines. While a contribution to the continuum from two-photon emission and the Balmer continuum exists at long UV wavelengths, the illuminating star is on the order of 40 times brighter at the shortest wavelengths than it is in the visible. Therefore, the Orion Nebula is a reflection nebula in the UV.

The same payload that obtained the UV spectra of two planetary nebulae was used to photograph the UV spectrum of a region of the Orion Nebula. These Aerobee rocket flights used a STRAP IV pointing system to position the planetaries NGC 7027 (Bohlin, Marioni, and Stecher 1975) and NGC 7662 (Bohlin, Harrington, and Stecher 1978) within the 17' \times 24' field of view. Since the pointing errors with the STRAP IV system are only a few minutes of arc, observation of

the extensive nebulosity in the Trapezium region of Orion was possible. For this purpose, an entrance slit of $22'' \times 17'$ was placed at the focal plane of the telescope, creating a long-slit spectrograph with a wavelength resolution of 22 \AA FWHM and a spatial resolution of $14''$ along the slit.

The star HD 37042 (θ^2 Orionis B) appeared in the entrance slit, producing a narrow spectrum near the center of the spectrogram. The remainder of the image on film exhibits the spectrum of the diffuse nebula, which is primarily the continuous stellar spectrum of the O6ep star θ^1 Ori C scattered by the dust. The strong C IV multiplet at 1549 \AA , a common indicator of mass loss in O stars, is seen as a blueshifted absorption line in the nebular spectrum, implying that θ^1 Ori C is the main source of the observed continuous emission. In contrast to the rich emission-line spectrum in the visual, only the three emission lines of C III] at 1908 \AA , C II] at 2326 \AA , and [O II] at 2470 \AA are seen in the UV spectrum. The details of the observation and the data reduction are presented in the next two sections (§§ II and III). The physical significance of the observations are discussed in §§ IV and V.

II. OBSERVATIONS

The Aerobee 200 rocket was launched from the White Sands Missile Range at $03^{\text{h}}00^{\text{m}}$ UT on 1975 February 1. As in previous flights, the detector was a microchannel plate enclosed in a sealed tube with a semitransparent cesium telluride cathode. Fiber optics coupled the phosphor screen output to 35 mm Kodak IIa-O film. The plate scale is $46.46 \text{ \AA mm}^{-1}$ in the dispersion direction and $0.773' \text{ mm}^{-1}$ perpendicular to the dispersion. The location of the entrance slit on the sky is shown in Figure 1. The position angle is known to be $47^\circ \pm 0.5^\circ$ west of north from the constraints placed on the STRAP IV pointing system. The payload telescope and detector were used as an aspect camera to determine the location of the center of the slit. After completion of the prime science exposures, a drift scan at $10'' \text{ s}^{-1}$ was begun perpendicular to the slit and toward the northeast. Exposures of 10 s were taken during the drift scan. Final aspect was verified by time and position along the slit when the entrance aperture passed the stars HD 37062 and HD 37061, just off the edge of Figure 1.

III. DATA REDUCTION

a) Image Processing

The Orion spectral images are a considerably more complex problem in image processing than the earlier spectra of planetary nebulae. Instead of just one prime data frame, the Orion data is on three frames of 60 s exposure each. During each exposure the rocket pointing drifted at about $0.15'' \text{ s}^{-1}$ along the slit, requiring a shift of the images before addition. The two-dimensional nature of the Orion data, in contrast to the linear spectra of NGC 7027 and NGC 7662, is

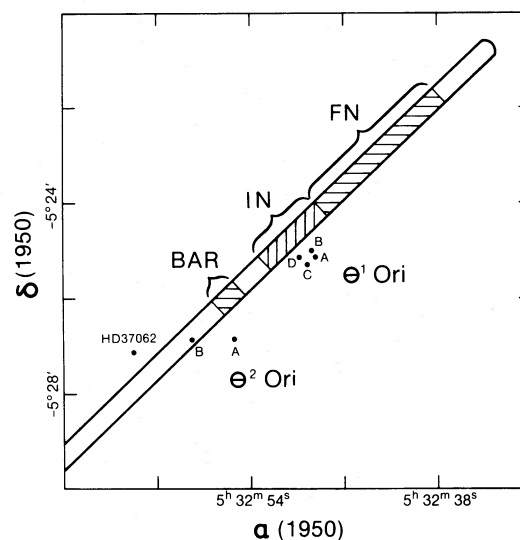


FIG. 1.—The position of the spectrograph slit on the sky together with the positions of the stars θ^1 Ori (the Trapezium) and θ^2 Ori. The areas along the slot corresponding to the BAR, IN (inner nebula), and FN (faint nebula) regions of the Orion Nebula are marked.

the greatest complication. In order to compare information at the same wavelength, but at different positions along the slit, the effects of cathode non-uniformity and vignetting must be removed.

The following set of sequential steps summarizes the Orion data reduction, but, at the same time, should typify the procedures required to fully analyze any astronomical data obtained using film and an image intensifier tube.

1. All of the flight film and calibration frames were scanned with a $75 \mu\text{m}$ square aperture on a PDS densitometer. This defines a pixel of an image.
2. The relation between relative exposure H and density D is determined from a set of frames having constant light input and known exposure times, assuming no reciprocity failure. The microchannel plate plus film detector system is expected to have no reciprocity failure, because each detected photon is amplified sufficiently to register on the film.
3. The background fog level of each frame is adjusted to the average value and the density converted to relative intensity.
4. Uniform illumination of tube alone defines the large- and small-scale cathode nonuniformities.
5. Long-slit spectra of a diffusing screen, uniformly illuminated by a deuterium continuum lamp determines the vignetting function, i.e., the relative sensitivity perpendicular to the dispersion. These spectral frames are divided by the uniformity frame of step (4) above in order to measure the vignetting and verify that it is the same to 10% from 1800 to 2800 \AA .
6. The uniform illumination from step (4) is multiplied by the smooth vignetting function of step (5) to produce the complete flat field correction for all wavelengths.

7. By dividing the individual flight frames from step (3) by the flat field of step (6), the instrumental signature is removed from the data. Prior to this step, small rotations of the images were done as necessary to register the images and account for small misalignment during the PDS scans.

8. The drift of the rocket pointing along the slit was 3 pixels during each of the three 60 s exposures. The individual exposures are shifted to compensate for the rocket motion.

9. In order to produce the best signal-to-noise ratio the three frames from step (8) are averaged.

10. The result of step (9) is displayed in Figure 2 (Plate 5) after further processing to enhance the visibility of the spectral features. Different regions along the slit have been scaled by three separate factors in order to make the full dynamic range of the result visible in Figure 2. Note the vertical row of three black dots at 1280 Å between the BAR and the inner nebula (IN) regions. The dot is a fixed blemish on the detector and, thus, the vertical separation measures the amount of image shift from step (8). The stellar spectrum would have been widened by the total separation of the dots, if the different shifts had not been applied.

11. The relative intensity along the slit is extracted in three 200 Å bands and presented in Figure 3. Note the systematic change in color from the inner nebula (IN) region through the fainter nebulosity (FN). The amount of instrumental scattered light from θ^2 Ori B, which lies within the slit, was determined knowing the instrumental point spread function from another spectrum of the point source β Ori. The amount of scattered light at the extreme point closest to θ^2 Ori B in Figure 3 is about 20%, falling to less than 10% at the distance of the BAR and beyond. Any scattered light from the Trapezium stars, which lie outside the slit, is significantly less.

b) Absolute Calibration

Once the PDS density D has been linearized to relative intensity H , the values of H are equivalent to linear counts per pixel in an ideal detector and can be

used to define an absolute calibration. The data reduction steps continue using spectra extracted as a function of wavelength from the average image of step (9).

12. The response H to the star θ^2 Ori B is used to define the absolute calibration for a point source on the *IUE* scale (Bohlin *et al.* 1980). This is possible because *IUE* observations of θ^2 Ori B (R. C. Bohlin and B. D. Savage, in preparation) have determined the absolute flux for θ^2 Ori B in the rocket UV.

13. The absolute calibration for surface brightness S can be found from the calibration for a point source using the known slit width and the plate scale, which yields a value of $2.85 \times 10^{-10} \text{ sr}^{-1} \text{ pixel}^{-1}$.

14. The best check of overall accuracy of the rocket data is from a comparison of the absolute value of S in the BAR region to a measurement in the same region by *IUE*. The maximum difference between the two determinations is 10%.

15. In order to compare the rocket measurements of S to the source of the illumination, the *IUE* flux for θ^1 Ori C (R. C. Bohlin and B. D. Savage, in preparation) is introduced. This comparison can be made directly because the rocket data have been calibrated using the *IUE* absolute flux scale.

16. The absolute flux of θ^2 Ori B and of three regions of extended nebulosity are extracted from the composite image and compared to θ^1 Ori C in Figure 4.

c) Results

i) Carbon and Oxygen Lines

Table 1 contains the measured emission-line strengths of the identified nebular features, along with the relative mean column densities for three regions of the nebula. The three regions along the slit are defined in Figures 1 and 2. They are the BAR, generally believed to be an ionization front, which is reddish on color photographs of Orion; the inner nebula (IN), where the nebulosity has a local intensity maximum nearest the Trapezium; and the fainter nebulosity (FN) northwest of the Trapezium. The $N(\text{C III})/N(\text{O II})$ and $N(\text{C II})/N(\text{O II})$ column density ratios for

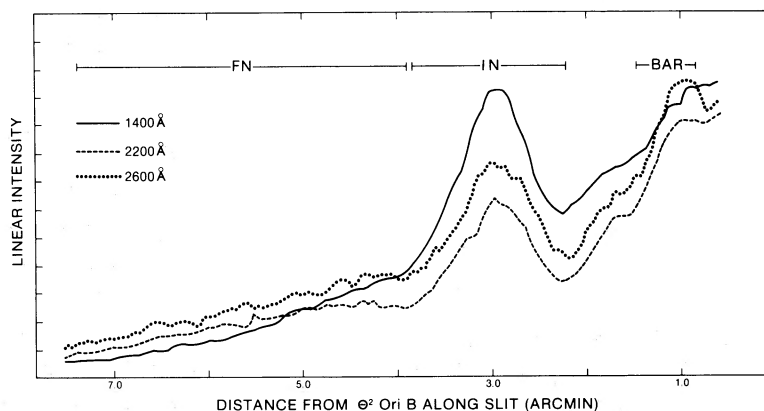


FIG. 3.—Relative intensity along the slit for 200 Å bandpasses centered on wavelengths 1400 Å, 2200 Å, and 2600 Å. Distance is measured from θ^2 Ori B in minutes of arc along the slit. Curves are scaled arbitrarily.

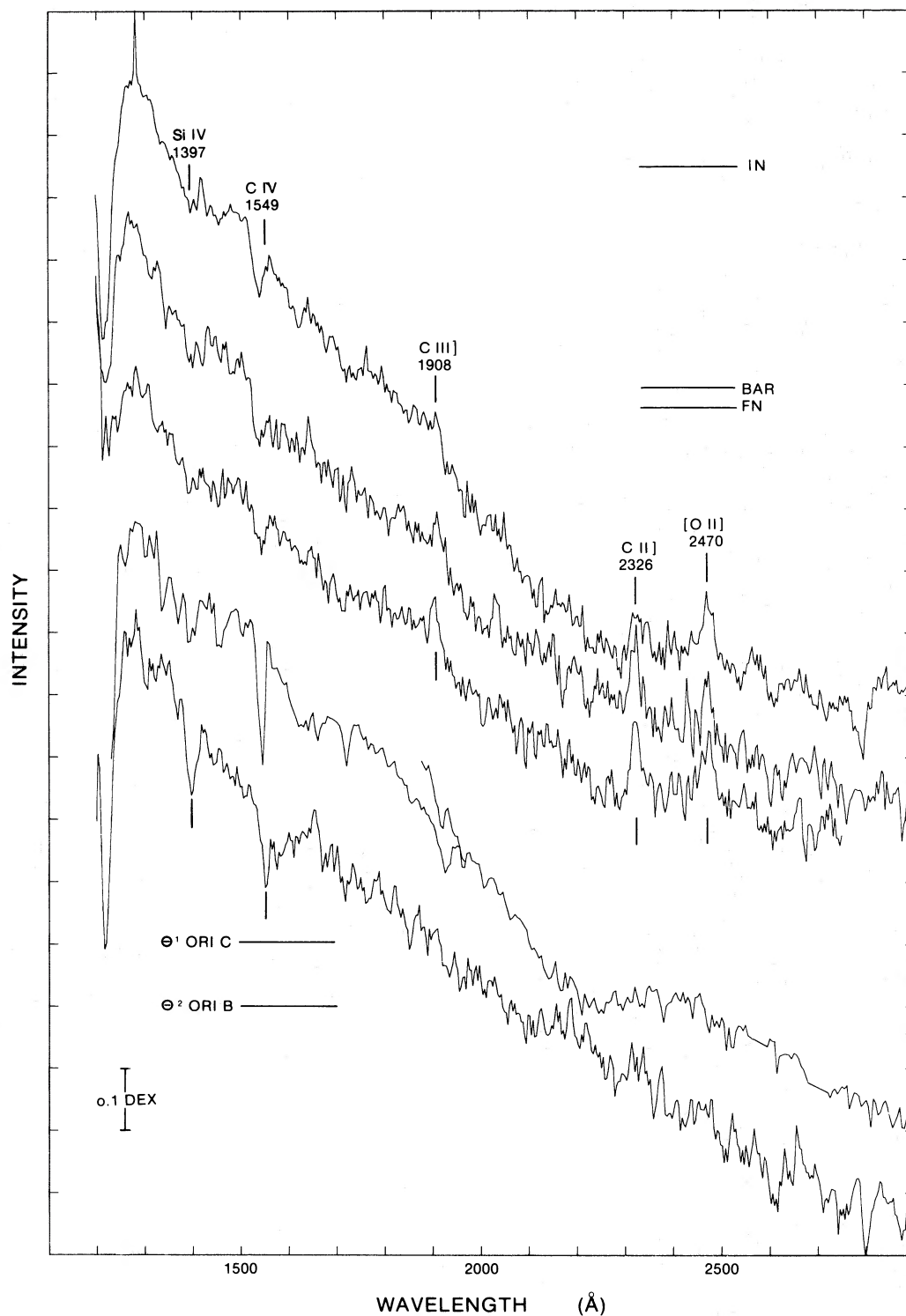


FIG. 4.—Rocket spectra of BAR, IN, FN, and θ^2 Ori B, together with IUE spectrum of θ^1 Ori C in absolute units on a logarithmic scale. The horizontal lines at the upper right indicate the level corresponding to 10^{-3} ergs cm^{-2} \AA^{-1} sr^{-1} (BAR, IN) or $10^{-3.5}$ ergs cm^{-2} s^{-1} \AA^{-1} sr^{-1} (FN). The horizontal lines at the lower left indicate the level corresponding to $10^{-9.5}$ ergs cm^{-2} s^{-1} \AA^{-1} (θ^1 Ori C) or 10^{-10} ergs cm^{-2} s^{-1} \AA^{-1} (θ^2 Ori B). The curves have the same order from top to bottom in the figure as their corresponding level indicators.

TABLE 1
EMISSION-LINE STRENGTHS AND ABUNDANCES OF
CARBON AND OXYGEN

Emission-Line Strengths and Abundance Ratios	BAR	IN	FN
$S(1908 \text{ \AA}, \text{C III})^a$	12	5.2	4.5
$S(2326 \text{ \AA}, \text{C II})^a$	20	9.8	5.5
$S(2470 \text{ \AA}, \text{O II})^a$	11	8.1	4.3
$N(\text{C III})/N(\text{O II})$	0.18	1.22	0.74
$N(\text{C II})/N(\text{O II})$	1.01	1.06	0.56
$N(\text{O III})/N(\text{O II})$	0.10	2.04	0.69
$N(\text{C})/N(\text{O})^b$	1.08	0.75	0.76

^a $10^{-4} \text{ ergs cm}^{-2} \text{ s}^{-1} \text{ sr}^{-1}$.

^b $N(\text{C})/N(\text{O})$ for the Sun is 0.56 (Lambert 1978).

each region are computed using the equation

$$\frac{N(i)}{N(\text{O II})} = \frac{\lambda}{2470 \text{ \AA}} \frac{q(\text{O II})}{q(i)} \frac{S(\lambda)}{S(2470)}$$

where $\lambda = 2326 \text{ \AA}$ for $i = \text{C II}$ and $\lambda = 1908 \text{ \AA}$ for $i = \text{C III}$. Here $S(\lambda)$ is the measured specific intensity of the emission line of wavelength λ and $q(i)$ is the collisional excitation rate of the transition at wavelength λ for ion i . In the case of O II the rate is modified to take into account collisional de-excitation of the levels giving rise to the $\lambda 3727$ doublet.

Peimbert and Torres-Peimbert (1977) have determined temperatures characteristic of the low- and high-ionization regions of the nebula as a function of position using optical transitions of $[\text{N II}]$ and $[\text{O III}]$. We have used these temperatures in determining values for $q(i)$, assuming that the $[\text{N II}]$ temperature is appropriate for C II and $[\text{O II}]$ and the $[\text{O III}]$ temperature is appropriate for C III . The C/O abundance ratios for each of the three regions of the nebula is determined assuming $N(\text{C}) = N(\text{C II}) + N(\text{C III})$ and $N(\text{O}) = N(\text{O II}) + N(\text{O III})$, using the $N(\text{O III})/N(\text{O II})$ abundance ratio appropriate for that region as determined by Peimbert and Torres-Peimbert (1977). The collision strengths and transition probabilities for $[\text{O II}]$ are from Pradhan (1976) and Garstang (1968), respectively. The C II and C III collision strengths are those of Jackson (1973) and Dufton *et al.* (1978), respectively. The estimated error in the line strengths is 30% due primarily to uncertainty in the continuum level. No correction for differential reddening for the three lines has been applied, but it is less than 20% in the ratio of line strengths. A value for the mean square temperature fluctuation $t^2 = 0$ is used for results shown in Table 1. Because of the large energy required to excite the 1908 \AA doublet, $N(\text{C III})/N(\text{O II})$ is quite sensitive to the value of t^2 . For a reasonable value of $t^2 = 0.035$, a maximum increase of 60% occurs for the ratio of C to O in the FN region. Thus, the uncertainty in t^2 dominates the errors in the results; and since t^2 may vary as a function of position in the nebula, the apparent difference in the C/O abundance ratio among the three regions is probably not significant. However, an overabundance with respect to the Sun of C relative

to O of up to a factor of 2 is suggested in Orion. In contrast, the solar C/O abundance of 0.6 was found by Peimbert and Torres-Peimbert (1977) from weak permitted lines of C II .

ii) Continuum

The result that the UV continuum in Orion is primarily scattered light from the dust is consistent with the findings of O'Dell and Hubbard (1965), Peimbert and Goldsmith (1972), and Schiffer and Mathis (1974) that in the visible most of the continuum emission of the Orion Nebula is due to dust-scattered light. Perinotto and Patriarchi (1980) estimate that less than 5% of the far-UV continuum of the Orion Nebula results from atomic emission processes.

In the near-UV the proportion of atomic continuum emission must be expected to be somewhat higher. Using the emission coefficients calculated by Brown and Mathews (1970), the ratio of scattered to atomic continuum at 4580 \AA of Schiffer and Mathis (1974), and the calculated shape of the atomic continuum of Perinotto and Patriarchi (1980), we estimate that 25% of the observed continuum at 2800 \AA is of atomic origin, declining to 15% at 2100 \AA and 4% at 1300 \AA . The relative nebular surface brightness, expressed as $\log(S/F)$, where F is the flux from $\theta^1 \text{ Ori C}$ received at Earth in units of $[\text{ergs cm}^{-2} \text{ s}^{-1} \text{ \AA}^{-1}]$ and S is the nebular intensity in the same units per steradian, is shown for the three regions denoted as IN, BAR, and FN in Figure 5. The upper points for each region were calculated using the total observed nebular intensity, the lower dashed lines are based on the intensities corrected for the atomic contribution.

It is noteworthy that these ratios are essentially featureless. The slight bump at 2200 \AA could be caused by the patchiness of the extinction in the Trapezium, where $\theta^1 \text{ Ori C}$ would have a slight excess of extinction compared to the nebula. The nebular color in the UV shortward of 2500 \AA is dependent on the projected distance with respect to $\theta^1 \text{ Ori}$, with IN exhibiting a color bluer than that of the star, BAR displaying essentially neutral color, while FN has a red color compared with $\theta^1 \text{ Ori C}$. This behavior is apparently typical of UV reflection nebulae and has been seen in similar fashion in the Merope nebula by Andriess, Piersma, and Witt (1977) and in the large Orion reflection nebula by Witt and Lillie (1978). It is also remarkable that the level of $\log(S/F)$ for IN and BAR throughout the UV is essentially the same as that found by Schiffer and Mathis (1974) at 4580 \AA for the central Orion Nebula. Their relative surface brightness reduced to an offset distance of $38''$, the approximate distance of IN from $\theta^1 \text{ Ori C}$, is $\log(S/F)_{4580} = 6.0$. In this respect, then, the Orion Nebula shows a marked difference with respect to the Merope nebula (Witt 1977), where $\log(S/F)_{100''}$ increases by 0.5 between the wavelengths 4690 and 1550 . This difference must be understood partly as a result of a different star-nebula geometry, and possibly partly as a true difference in the nature of the grains in the Orion Nebula.

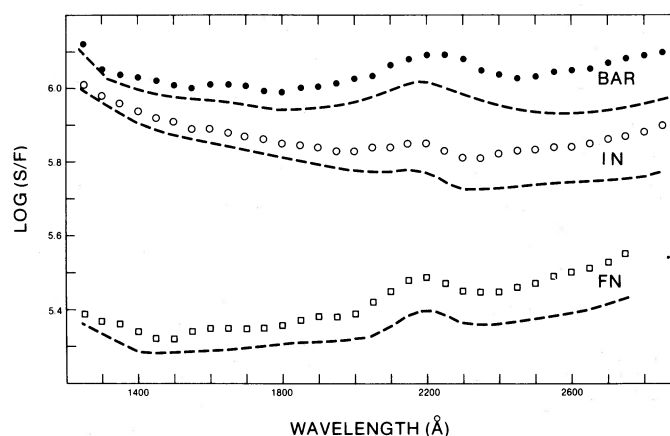


FIG. 5.—Surface brightness divided by observed stellar flux of θ^1 Ori C for BAR, IN, and FN (sr^{-1}) on a logarithmic scale vs. wavelength. Curves have been smoothed over 50 Å intervals. The upper symbols and lower curves (*dashed lines*) are uncorrected and corrected for atomic continuum emission, respectively.

The study of reflection nebulae in the UV offers several distinct advantages. In most cases the nebulae are illuminated by early-type stars of high luminosity, making them bright objects in the UV. The geometric relationship between source and scatterers will be assumed to be constant with wavelength. Most importantly, because of the structure in the UV extinction curve, one can define three wavelengths, two located on either side of the 2200 Å extinction “hump” and one on the rising part of extinction curve shortward of 1600 Å, where the optical depth per unit length in the nebula is the same. If the extinction curve for θ^1 Ori is valid for the dust in the Orion Nebula as a whole, then these three wavelengths are at 2440 Å, 1800 Å, and 1230 Å (Savage 1973). Differences in the relative surface brightness and changes of color with position measured at these three wavelengths are not a result of changes of the optical depth with wavelength as is the case with observation in the visible. Instead, such changes are the result of actual differences in the scattering properties of the nebular grains found at the three critical wavelengths.

In Figure 6 we show the variation of (S/F) , normalized to unity at 2440 Å, for the regions IN, BAR, and FN. The measurement in the far-UV was made at 1300 Å rather than at 1230 Å in order to avoid confusion with $\text{L}\alpha$. Since the θ^1 Ori extinction curve (Savage 1973) is essentially flat in this region, this change in wavelength is not significant enough to invalidate the outlined approach. Figure 6 contains both the ratios $(S/F)_\lambda / (S/F)_{2440}$ for the total (scattered atomic) continuum as the lower set of curves, and for the continuum corrected for the atomic contribution as the upper set of curves. The true curves will likely fall near the upper limit of the three shaded regions.

We find that the values of (S/F) at the three wavelengths of constant optical depth are different from one another for a given region as well as from

region to region. From this we can conclude the following: if the scattering phase function of the grains were identical at the three critical wavelengths, the different values of (S/F) at 1800 Å and 1300 Å relative to that at 2440 Å would be indicative of albedo changes. In that case, however, the shape of the three curves in Figure 6 would have to be identical to each other. Since they differ significantly, we *must conclude* that the scattering phase function changes its shape through the wavelength region from 2440 Å to 1300 Å. An albedo variation may or may not be present as well,

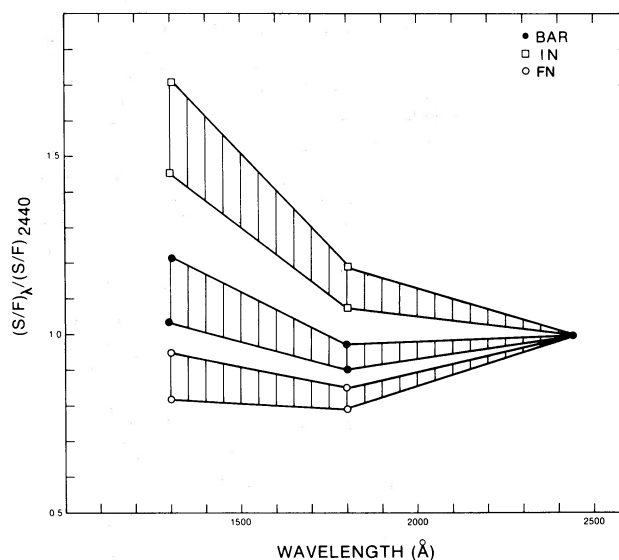


FIG. 6.—The variation of (S/F) for the three parts of the nebula as a function of wavelength for the 3 special wavelengths of constant optical depth normalized to unity at 2440 Å. The spread in the points represents the limits on the correction for the atomic continuum. The true curves are thought to be near the upper limit of the 3 cross-hatched regions. We interpret the variation of (S/F) as requiring a scattering phase function change with wavelength. An albedo variation may or may not be present as well.

a question which can only be resolved with a knowledge of the detailed geometry of the three regions involved.

IV. THE STRUCTURE OF THE ORION NEBULA

The geometry of the Orion Nebula is complex. There appears to be agreement that θ^1 Ori is located about 0.1 pc in front of a dense, neutral molecular cloud with the visible H II region resulting from ionization of gas streaming away from the neutral cloud (Zuckermann 1973; Balick, Gammon and Hjellming 1974). Both the ionizing stars and the ionization front are advancing into the neutral cloud (Pankonin, Walmsley, and Harwit 1979). Radiation pressure and/or a stellar wind originating in θ^1 Ori C are believed to create a bubble devoid of dust and most gas with a radius of about 0.15 pc; but the picture is immensely complicated by the apparent presence of partially ionized dense globules in the inner Orion Nebula, making the distribution along any line of sight extremely nonhomogeneous on a very small scale (Laques and Vidal 1979; Isobe 1979). Schiffer and Mathis (1974) have provided arguments for a shell model with a relatively large dust-free region with a diameter of nearly 1 pc ($\sim 7'$) based on the observed distribution of the scattered continuum at visual wavelengths. However, the high-resolution scans of the Orion Nebula by Münch and Persson (1971) provided evidence for the significant spatial fine structure and lack of symmetry in the light distributions with respect to θ^1 Ori, which would make the adoption of a simplified geometrical model such as that of Schiffer and Mathis (1974) not advisable for the explanation of the data provided in this rocket experiment. It appears safe to conclude that there is a significant amount of dust present both in front of and behind θ^1 Ori. The optical depth to θ^1 Ori C is uncertain as a result of its highly abnormal reddening curve, but may be of the order of $\tau \approx 4$ for the UV based on the data discussed by Schiffer and Mathis (1974) and the reddening curve provided by Savage (1973). It is believed that most of this optical depth arises within the nebula itself (Münch and Persson 1971; Schiffer and Mathis 1974). The observed scattered continuum light seen by our experiment is therefore the result of significant multiple scattering. The multiplicity of scattering (Witt and Oshel 1977) for light seen along a line of sight near θ^1 Ori such as our IN, would therefore be of the same order as the value of τ . Since significant multiple scattering has the effect of enhancing the influence of any albedo variation with wavelength upon the observed relative nebular surface brightness, the absence of any large modulation of (S/F) in Figure 5 strongly suggests that the dust in the Orion Nebula has essentially constant albedo throughout the UV. This is in contrast to the albedo variation found by Lillie and Witt (1976) for interstellar dust in general, where a minimum at 2200 Å corresponding to the strong extinction hump at the same wavelength is present.

V. RADIATIVE TRANSFER CONSIDERATIONS

In view of the structural complexity of the Orion Nebula we prefer not to adopt a specific geometrical model, but rather pursue general considerations applicable to the three special wavelengths of constant optical depth. Aside from factors involving the optical depth which cancel each other, we may write

$$\frac{(S/F)_\lambda}{(S/F)_{2440}} \approx \frac{a^n(\lambda)}{a^n(2440)} \frac{\int_{\alpha_1}^{\alpha_2} \phi[\alpha, g(\lambda)] \sin^2 \alpha d\alpha}{\int_{\alpha_1}^{\alpha_2} \phi[\alpha, g(2440)] \sin^2 \alpha d\alpha}, \quad (1)$$

where S and F are the nebular intensity and the stellar flux, $a(\lambda)$ is the grain albedo, $\phi(\alpha, g)$ is the phase function with α the scattering angle, and n the multiplicity of scattering. The values for λ are 1800 Å or 1300 Å. In light of the arguments advanced in § IV we shall assume that $a^n(\lambda)/a^n(2440) \approx 1$.

A versatile analytical form for an asymmetric phase function has been introduced by Henyey and Greenstein (1941):

$$\phi(\alpha, g) = [(1 - g^2)/4\pi] \times (1 + g^2 - 2g \cos \alpha)^{-3/2}, \quad (2)$$

where $g \equiv \langle \cos \alpha \rangle$ is the so-called asymmetry factor. The parameter g measures the degree to which radiation is scattered into the forward hemisphere compared to the back hemisphere and ranges from +1 for complete forward scattering through 0 for isotropic scattering to -1 for complete backscattering. The empirical values of g determined here are primarily indicators of the average size of the particles responsible for the scattering at the wavelengths considered. Wavelength sized particles generally scatter strongly in the forward direction, whereas particles small compared to the wavelengths have a nearly isotropic phase function.

To more adequately describe the composite grain mixture required to explain properties of interstellar grains both in the visible and in the UV, we prefer to use a superposition of two Henyey-Greenstein phase functions of the form (Irvine 1965):

$$P(\alpha, g_{\text{eff}}) = \gamma \phi(\alpha, g_1) + (1 - \gamma) \phi(\alpha, g_2), \quad (3)$$

where

$$g_{\text{eff}} = \gamma g_1 + (1 - \gamma) g_2. \quad (4)$$

In Figure 7 we have plotted the arguments of the contribution function integral (1) for the values of $g_1 = 0.7$, $g_2 = 0$; and $\gamma = 1, 0.71, 0.36$, and 0, as a function of the scattering angle α , using this composite phase function P to replace ϕ . These curves indicate the contribution made by different elements of an optically thin, homogeneous nebula to the scattered intensity seen along a line of sight. The offset from the source of illumination and the scattering angle uniquely define the relative location of the scattering element. In an optically thick nebula where most of the scattering is from dust in front of the star, light scattered at deeper levels suffers additional extinction by foreground dust, while the dust close to the front

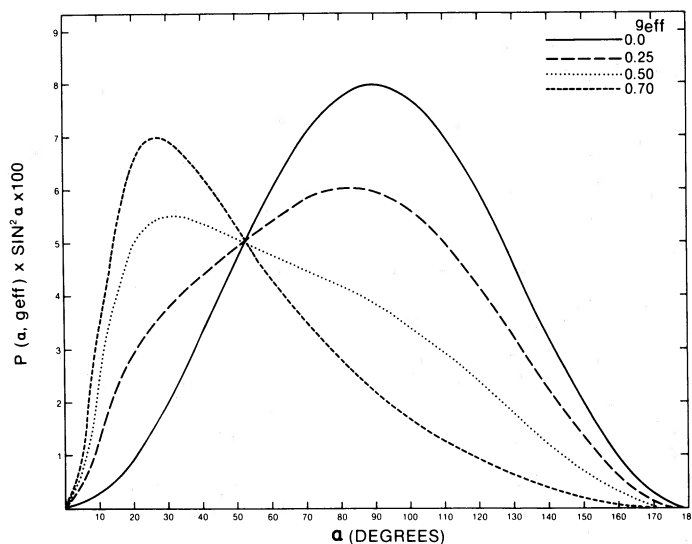


FIG. 7.—The arguments of the contribution function integral, $P(\alpha, g_{\text{eff}}) \sin^2 \alpha \times 100$, plotted as a function of the scattering angle in degrees. $P(\alpha, g_{\text{eff}})$ is a superposition of 2 Henyey-Greenstein phase functions used to represent a composite grain mixture.

surface is illuminated by starlight reduced by a similar amount of extinction, so that the ratio of contribution function integrals as given by equation (1) may still describe reasonably well the observations in the case of an optically thick nebula with g_{eff} varying with wavelength.

Different geometric arrangements of the dust distribution with respect to the source of illumination may be defined by specifying the limits α_1 and α_2 of the active range of scattering angles. Figure 3 shows the ratios Q of the contribution function integrals (1) for several ranges of the scattering angle, nor-

malized to $g_{\text{eff}} = 0.5$. According to equation (1), $Q = (S/F)_\lambda / (S/F)_{2440}$ provided the albedo $a(\lambda) = a(2440)$. If $\alpha_1 < \alpha_2 \leq 90^\circ$, the scattering material is confined to the space between the star and the observer, and if $\alpha_1 < 90^\circ < \alpha_2$, dust lies both in front of and behind the source of illumination. Also shown in Figure 8 are the ratios $(S/F)_{1300} / (S/F)_{2440}$ for IN and FN. As discussed at the end of § III the data shown in Figure 6 could only be understood if the phase functions at 1800 Å and at 1300 Å differ from the phase function at 2440 Å. If we assume for the moment that $g_{\text{eff}}(2440) = 0.5$, typical of results in reflection

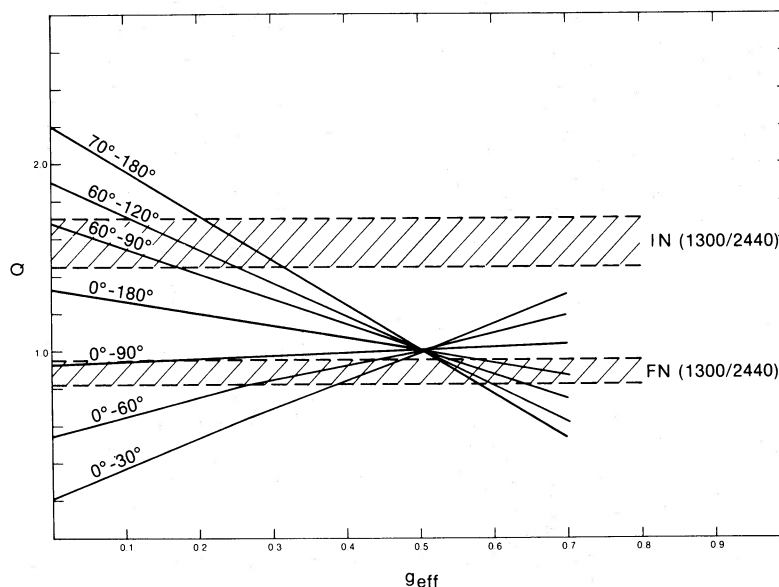


FIG. 8.—The ratios of the contribution function integrals Q as a function of the effective asymmetry factor for several ranges of the scattering angle. Also plotted are $(S/F)_{1300} / (S/F)_{2440}$ for IN and FN, which are equal to Q , if the albedo at 1300 Å is the same.

nebulae (Witt 1977), the question remains whether the phase function in the far-UV is more or less forward throwing, i.e., $g_{\text{eff}}(1300) > g_{\text{eff}}(2440)$ or $g_{\text{eff}}(1300) < g_{\text{eff}}(2440)$. The answer depends on the prevailing geometry at IN and FN. If at IN the scattering dust is relatively close to the star, either completely in front as given by the case $(\alpha_1, \alpha_2) = (60^\circ, 90^\circ)$, or both in front and behind as specified by $(\alpha_1, \alpha_2) = (60^\circ, 120^\circ)$ and $(70^\circ, 180^\circ)$, the answer is clearly $g_{\text{eff}}(1300) < g_{\text{eff}}(2440)$, with an approximate value $g_{\text{eff}}(1300) = 0.25 \pm 0.10$. In this case the scattering of FN would have been limited to scattering angles between 0° and 90° . If, in fact, the schematic geometry of the Orion Nebula resembles that shown by Pankonin, Walmsley, and Harwit (1979) and by Dopita, Isobe, and Meaburn (1975) with θ^1 Ori located in a bay of a dense, molecular cloud, this range of scattering angles, i.e., 0° to 90° , is the only one possible for FN.

Alternatively, we would have to conclude that $g_{\text{eff}}(1300) > g_{\text{eff}}(2440)$ if the material at IN could be shown to be confined to a shell well in front of θ^1 Ori permitting scattering only at angles $\alpha \leq 30^\circ$, and if the material at FN had a distribution allowing scattering over a wide range of scattering angles, including a significant amount of back scattering.

A further constraint in these considerations is the fact mentioned in § III that the relative nebular surface brightness (S/F) of the inner Orion Nebula in the UV is essentially the same as that found in the visible. Since

the optical depth of the Orion Nebula is measurably higher in the UV, this implies that the overall scattering efficiency of the nebular dust in the direction of Earth is actually lower in the UV than in the visible. For a constant or increasingly forward scattering phase function this probably implies a noticeably lower albedo in the UV compared to the visible, while an essentially constant albedo as suggested in § IV would require a phase function which changes to a more isotropic form, i.e., $g_{\text{eff}}(1300) < g_{\text{eff}}(2440)$.

While the present observations tend to slightly favor the latter case, it will clearly require a more detailed study of the spatial distribution of the scattered continuum at both visible and ultraviolet wavelengths to resolve the question of the ultraviolet scattering properties of the Orion Nebula dust. Since the Orion extinction curve is anomalous, the detailed optical properties of grains in Orion probably differ from those in the normal interstellar medium.

We thank the launch support crew for Aerobee 26.027 including G. Baker, A. Stober, and T. Collinson for another flawless performance of the entire system. We are appreciative of the help in data reduction from Dr. Theresa Nagy and Jan Niebur. Dr. D. A. Klinglesmith implemented the VICAR system, which was used for a large part of the image processing. One of us (A. N. W.) was supported by NASA grant NSG 7431.

REFERENCES

- Andriessse, C. D., Piersma, Th. R., and Witt, A. N. 1977, *Astr. Ap.*, **54**, 841.
 Balick, B., Gammon, R. H., and Hjellming, R. M. 1974, *Pub. A.S.P.*, **86**, 616.
 Bohlin, R. C., Harrington, J. P., and Stecher, T. P. 1978, *Ap. J.*, **219**, 575.
 Bohlin, R. C., Holm, A. V., Savage, B. D., Snijders, M. A. J., and Sparks, W. M. 1980, *Astr. Ap.*, in press.
 Bohlin, R. C., Marionni, P. A., and Stecher, T. P. 1975, *Ap. J.*, **202**, 415.
 Brown, R. L., and Mathews, W. G., 1970, *Ap. J.*, **160**, 939.
 Dopita, M. A., Isobe, S., and Meaburn, J. 1975, *Ap. Space Sci.*, **34**, 91.
 Dufton, P. L., Berrington, K. A., Burke, P. E., and Kingston, A. E. 1978, *Astr. Ap.*, **62**, 111.
 Garstang, R. H. 1968, in *IAU Symposium 34, Planetary Nebulae*, ed. D. E. Osterbrock and C. R. O'Dell (Dordrecht: Reidel), p. 143.
 Henyey, L. G., and Greenstein, J. L. 1941, *Ap. J.*, **93**, 70.
 Irvine, W. M. 1965, *Ap. J.*, **142**, 1563.
 Isobe, S. 1979, preprint.
 Jackson, A. R. G. 1973, *M.N.R.A.S.*, **165**, 53.
 Lambert, D. L. 1978, *M.N.R.A.S.*, **182**, 249.
 Laques, P., and Vidal, J. L. 1979, *Astr. Ap.*, **73**, 97.
 Lillie, C. F., and Witt, A. N. 1976, *Ap. J.*, **208**, 64.
 Münch, G., and Persson, S. E. 1971, *Ap. J.*, **165**, 241.
 O'Dell, C. R., and Hubbard, W. B. 1965, *Ap. J.*, **142**, 591.
 Pankonin, V., Walmsley, C. M., and Harwit, M. 1979, *Astr. Ap.*, **75**, 34.
 Peimbert, M., and Goldsmith, D. W. 1972, *Astr. Ap.*, **19**, 398.
 Peimbert, M., and Torres-Peimbert, S. 1977, *M.N.R.A.S.*, **179**, 217.
 Perinotto, M., and Patriarchi, P. 1980, *Ap. J. (Letters)*, **235**, L13.
 Pradhan, A. K. 1976, *M.N.R.A.S.*, **177**, 31.
 Savage, B. D. 1973, in *IAU Symposium 52, Interstellar Dust and Related Topics*, ed. J. M. Greenberg and H. C. van de Hulst (Dordrecht: Reidel), p. 21.
 Schiffer, F. H., III, and Mathis, J. S. 1974, *Ap. J.*, **194**, 597.
 Witt, A. N. 1977, *Pub. A.S.P.*, **89**, 750.
 Witt, A. N., and Lillie, C. F. 1978, *Ap. J.*, **222**, 909.
 Witt, A. N., and Oshel, E. R. 1977, *Ap. J. Suppl.* **35**, 31.
 Zuckerman, B. 1973, *Ap. J.*, **183**, 863.

R. C. BOHLIN and T. P. STECHER: NASA, Goddard Space Flight Center, Code 681, Greenbelt, MD 20771

J. K. HILL: Systems and Applied Sciences Corporation, 6811 Kenilworth Avenue, Riverdale, MD 20840

A. N. WITT: Ritter Observatory, University of Toledo, Toledo, OH 43606

ORION NEBULA

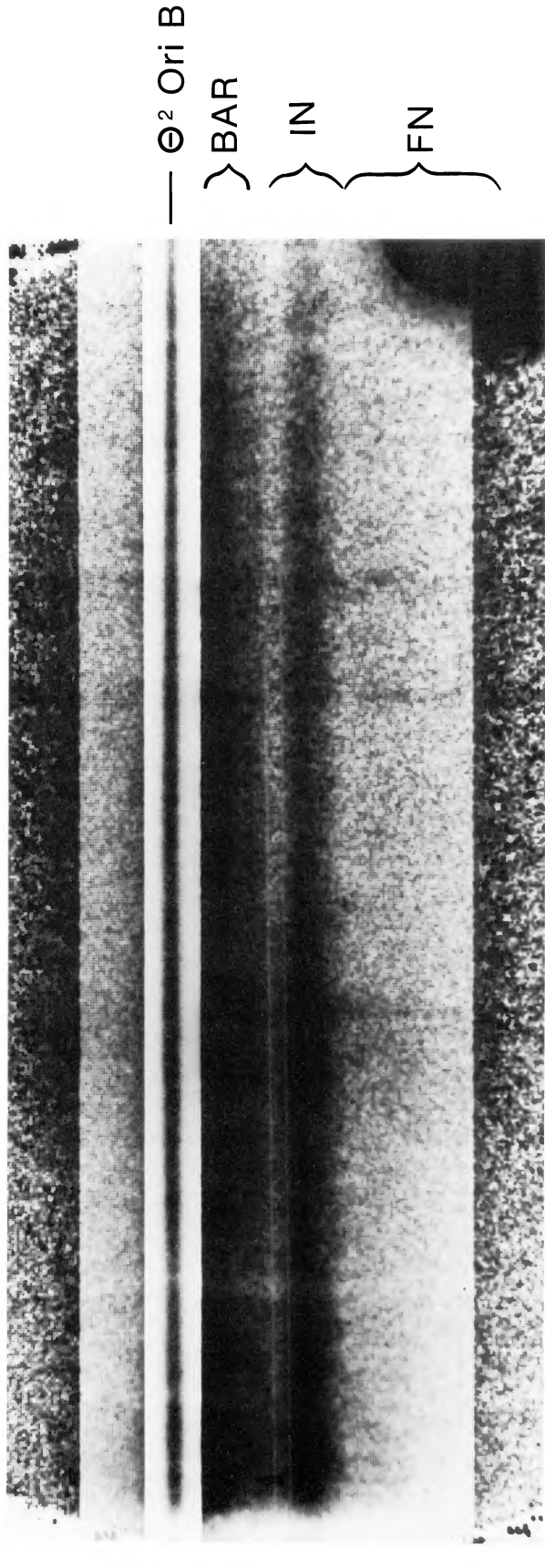


FIG. 2.—The final product of image processing steps (1) to (10). The region of the slit spectrogram around the star θ^2 Ori B is scaled by a factor of 300 with respect to the top and bottom areas of the figure. The diffuse nebulosity above and below the star is scaled by 6 with respect to the outer parts, which show mostly the noise level of the data. The 3 spatial regions discussed in the text and noted in Fig. 1 are marked with curly brackets. The 3 prominent absorption lines are at the shorter-wavelengths, with Si IV obvious only in the B0.5 V star θ^2 Ori B. The 3 longer-wavelength features indicated are in emission from the nebulosity.
 BOHLIN, HILL, STECHER, AND WITT (see page 139)